Wave energy associated with the variability of the stratospheric polar vortex

M. L. R. Liberato*, J. M. Castanheira**, L. de la Torre†

C. C. DaCamara†† and L. Gimeno†

*University of Trás-os-Montes e Alto Douro, Physics Dept., Portugal

**CESAM, University of Aveiro, Portugal

†Faculty of Sciences of Ourense, University of Vigo, Spain

††University of Lisbon, CGUL, IDL, Portugal

January 4, 2007

Journal of the Atmospheric Sciences (Revised at October 19, 2006)

Corresponding author:

J. M. Castanheira

Department of Physics, University of Aveiro

3810-193 Aveiro – PORTUGAL

E-mail: jcast@fis.ua.pt

Abstract

A study is performed on the energetics of planetary wave forcing associated with the variability of the Northern winter polar vortex. The analysis relies on a 3-Dimensional normal mode expansion of the atmospheric general circulation that allows partitioning the Total (i.e. Kinetic + Available Potential) atmospheric energy into the energy associated with Rossby and inertio-gravity modes with barotropic and baroclinic vertical structures. The analysis mainly departs from traditional ones in what respects to the wave forcing, which is here assessed in terms of Total energy amounts associated with the waves instead of heat and momentum fluxes. Such an approach provides a sounder framework than traditional ones based on EP flux diagnostics of wave propagation and related concepts of refractive indices and critical lines, which are strictly valid only in the cases of small-amplitude waves and in the context of the WKBJ approximation.

Positive (negative) anomalies of the energy associated with the first two baroclinic modes of the planetary Rossby wave with zonal wavenumber 1 are followed by downward progression of negative (positive) anomalies of the vortex strength. A signature of the vortex vacillation is also well apparent in the lagged correlation curves between the wave energy and the vortex strength. The analysis of the correlations between individual Rossby modes and the vortex strength further contributed to confirm the result from linear theory that the waves which force the vortex are those associated with the largest zonal and meridional scales.

The two composite analyses of stratospheric sudden warming (SSW) events of the displacement and split types have revealed different dynamics. SSWs of displacement type are forced by positive anomalies of the energy associated with

the first two baroclinic modes of planetary Rossby waves with zonal wavenumber 1; SSWs of the split type are in turn forced by positive anomalies of the energy associated with the planetary Rossby wave with zonal wavenumber 2, and the barotropic mode appears as the most important component. In what respects to stratospheric final warming (SFW) events, obtained results suggest that the wave dynamics is similar to the one in SSW events of the displacement type.

1 Introduction

Several observational studies, performed over the last ten years, suggest that the stratosphere does not respond passively to tropospheric forcing but does play instead an important role in driving climate and weather variability down to the surface [e.g., *Baldwin and Dunkerton*, 1999, 2001; *Hartmann et al.*, 2000; *Thompson et al.*, 2002; *Perlwitz and Harnik*, 2004]. Such studies have naturally generated an increasing interest for a better understanding of the dynamics of the stratosphere-troposphere coupling, and several modelling studies were specifically devoted to the subject [e.g., *Kodera and Kuroda*, 2000; *Polvani and Kushner*, 2002; *Song and Robinson*, 2004].

Recently, a set of observational studies has focused on the daily evolution of strong vortex anomalies [*McDaniel and Black* , 2005], polar vortex intensification [*Limpasuvan et al.*, 2005], life cycle of stratospheric sudden warming (SSW) events [*Limpasuvan et al.*, 2004; *Nakagawa and Yamazaky* , 2006; *Charlton and Polvani*, 2006] and the evolution of stratospheric final warming (SFW) events [*Black et al.*, 2006].

In the above-mentioned studies as well as in many other studies, the analysis of the wave forcing of stratospheric polar vortex was performed within the traditional framework of Eliassen-Palm (EP) flux. However, the use of the EP flux as a diagnostic tool of wave propagation is strictly valid only in the case of small-amplitude waves. Frequent usage is also made of other concepts associated with EP flux diagnostics, such as refractive indices and critical lines, even though neither the WKBJ approximation relating refractive indices and critical lines to wave propagation nor the relation between wave propagation and EP flux are valid in the case of strongly nonlinear flows like those

that take place during stratospheric sudden warming events [*Thuburn and Lagneau*, 1999].

To our knowledge no studies have considered the wave forcing of the stratospheric polar vortex from the point of view of the energy associated with the forcing waves. The main goal of this work is therefore to perform a diagnostic study of the Total (i.e. Kinetic + Available Potential) energy associated with the planetary waves which force the vortex dynamics. The analysis is based on a 3-Dimensional (3-D) normal mode decomposition of the atmospheric global circulation, which is partitioned into planetary Rossby waves and inertio-gravity waves, both types of waves possessing barotropic and baroclinic vertical structures. Time changes in the energy associated with each wave component may then be related with the observed vortex variability. It is worth emphasizing that instead of being restricted to the extratropical region, the analysis is here applied to the global atmosphere, and the circulation components are selected based on 3-D global functions. In this respect the connection between the polar stratospheric variability and the quasi biennial oscillation (QBO) is worth being emphasized [*Holton and Tan*, 1980; *Labitzke*, 1982], together with the model results of *Naito et al.* [2003] that have revealed a short-time cooling response to SSW events extending to the summer hemisphere, a feature that suggests the global character of SSW events. Another important feature of the method used here is that the energy is computed for the total circulation (i.e. climatology + anomaly) and therefore energy anomalies, associated with vortex variability, also include the contribution from the climatological waves, which should be taken into account when performing composite analysis.

The fact that the 3-D normal modes are eigensolutions of a set of primitive equations,

linearized with respect to a basic state at rest, may be pointed out as a shortcoming for their use. However, the normal modes form a complete basis to expand the global circulation, and the divergent or rotational character as well as the horizontal and vertical structures of the circulation projected onto them do not depend on the magnitude of the anomalies. On the other hand, as the normal mode approach allows decomposing the circulation both into zonal and meridional scales, we may assess the sensitivity of vortex wave forcing to both spatial scales. In this respect it is worth recalling that the linear wave theory shows that the vertical wave propagation depends both on zonal and meridional wave numbers [*Andrews et al.*, 1987]. However, EP flux diagnostic studies that may be found in the literature only show the dependence on the zonal scale by means of Fourier decompositions.

2 Method and data

2.1 3-D Normal Mode Scheme

An hydrostatic and adiabatic atmosphere may freely oscillate around a reference state at rest and the different oscillation modes may be characterized in terms of their respective vertical and horizontal structures. The horizontal structure of each mode is identical to the one of a free oscillation mode of an incompressible, homogeneous, hydrostatic and inviscid fluid over a rotating sphere. In such conditions, the primitive equations, linearized with respect to a basic state at rest having a pressure dependent temperature distribution $T_0(p)$, may be written in the following form

$$\frac{\partial u}{\partial t} - 2\Omega v \sin\theta + \frac{1}{a\cos\theta}\frac{\partial \phi}{\partial \lambda} = 0$$

$$\begin{aligned} \frac{\partial v}{\partial t} + 2\Omega u \sin\theta + \frac{1}{a}\frac{\partial \phi}{\partial \theta} &= 0 \\ \frac{\partial}{\partial p}\left[\frac{1}{S_0}\frac{\partial}{\partial p}\left(\frac{\partial \phi}{\partial t}\right)\right] - \nabla \cdot \mathbf{V} &= 0 \end{aligned} \tag{1}$$

where (λ, θ, p) are the longitude, latitude and pressure coordinates; ϕ, the perturbed geopotential field, is the deviation from the basic state geopotential profile $\Phi_0(p)$; and

$$S_0 = \frac{R}{p}\left(\frac{kT_0}{p} - \frac{\mathrm{d}T_0}{\mathrm{d}p}\right) \tag{2}$$

is the static stability parameter of the reference state. The remaining symbols in Eqs. (1) and (2) are the horizontal wind components (u, v), the earth's radius a, the angular speed of the earth's rotation Ω, the specific gas constant R, and the ratio k of the specific gas constant to the specific heat at constant pressure.

As model boundary conditions, it is assumed that $\omega = \mathrm{d}p/\mathrm{d}t$ vanishes as $p \longrightarrow 0$ and that the linearized geometric vertical velocity $w = \mathrm{d}z/\mathrm{d}t$ vanishes at a level of constant pressure, p_s, near the earth's surface.

The free oscillations – normal modes – of the linearized primitive equations (1) may be written in the form

$$\begin{bmatrix} u \\ v \\ \phi \end{bmatrix}_{msl,\alpha} = \exp(-i\,2\Omega\nu t)\, G_m(p)\, \exp(is\lambda)\, \mathbf{C}_m \cdot \begin{bmatrix} U(\theta) \\ iV(\theta) \\ Z(\theta) \end{bmatrix}_{msl,\alpha} \tag{3}$$

where $\mathbf{C}_m = \mathrm{diag}\left(\sqrt{gh_m}, \sqrt{gh_m}, gh_m\right)$ is a diagonal matrix of scaling factors, g being the earth's gravity and h_m the equivalent height. $G_m(p)$ is a separable vertical structure function and m is the respective vertical index. Each horizontal structure function is given by the product of a zonal wave with wavenumber s and a vector $[U(\theta), iV(\theta), Z(\theta)]^T_{msl,\alpha}$ which defines the meridional profile of the wave. Because the

meridional index l is associated with the number of zeros of the respective meridional profile, it may be regarded as an index of the meridional scale of the motion. Index $\alpha = 1, 2, 3$ respectively refers to westward traveling inertio-gravity waves, planetary Rossby waves and eastward traveling inertio-gravity waves. ν is a dimensionless frequency.

The normal modes form a complete orthogonal basis and therefore allow expanding the horizontal wind and the geopotential fields of the global atmosphere [e.g. *Daley*, 1991; *Tanaka*, 2003]

$$\begin{bmatrix} u \\ v \\ \phi \end{bmatrix} = \sum_{m=0}^{\infty} \sum_{s=-\infty}^{\infty} \sum_{l=0}^{\infty} \sum_{\alpha=1}^{3} w_{msl}^{\alpha}(t)\ G_m(p)\ \exp(is\lambda)\, \mathbf{C}_m \cdot \begin{bmatrix} U(\theta) \\ iV(\theta) \\ Z(\theta) \end{bmatrix}_{msl,\alpha} \tag{4}$$

The expansion coefficients, w_{msl}^{α}, are obtained by means of a vertical projection onto the vertical structure functions

$$(\hat{u}, \hat{v}, \hat{\phi})_m^T = \frac{1}{p_s} \int_0^{p_s} (u, v, \phi)^T G_m(p) dp, \tag{5}$$

followed by an horizontal projection onto the horizontal structure functions

$$w_{msl}^{\alpha} = \frac{1}{2\pi} \int_0^{2\pi} \int_{-\pi/2}^{\pi/2} (\mathbf{H}_{msl}^{\alpha})^* \, \mathbf{C}_m^{-1} \cdot (\hat{u}, \hat{v}, \hat{\phi})_m^T \cos\theta \, d\theta \, d\lambda. \tag{6}$$

We have assumed that the vertical structure functions, $G_m(p)$, and the horizontal structure functions, $\mathbf{H}_{msl}^{\alpha}(\lambda, \theta) = \exp(is\lambda)\ [U(\theta), iV(\theta), Z(\theta)]_{msl,\alpha}^T$, have unitary norms. Superscripts T and $(\,)^*$ respectively denote the transpose and the complex conjugate of the transpose.

It may be shown that the squared expansion coefficients are proportional to the Total (i.e., Kinetic + Available Potential) energy per unit area associated with the

respective modes [*Castanheira et al.*, 1999, and references therein]

$$E^{\alpha}_{msl}(t) = \frac{p_s h_m}{c_s} |w^{\alpha}_{msl}(t)|^2. \tag{7}$$

For $s = 0$, $c_0 = 4$ and E^{α}_{m0l} represents the total energy associated with a zonal symmetric α type mode with vertical and meridional indices (m, l), respectively, whereas for $s \geq 1$, E^{α}_{msl} represents the total energy of the complex conjugate pair of modes (α, msl) and $(\alpha, m(-s)l)$ and therefore $c_s = 2$.

2.2 Data and Data preparation

Projection onto 3-D normal modes

The data were obtained from the global reanalysis data set of the National Centers for Environmental Prediction-National Center for Atmospheric Research [NCEP/NCAR, *Kalnay et al.*, 1996]. We have used November to April daily means of the horizontal wind components (u, v) and of the geopotential height, available at 17 standard pressure levels from 1000 to 10 hPa, with a horizontal grid resolution of 2.5° lat. $\times\, 2.5^{\circ}$ long., covering the period 1958-2005. Each period from November to April is identified by the year to which January belongs.

We have projected the data onto the normal modes of the NCEP/NCAR reference atmosphere, which allows partitioning the atmospheric circulation into one barotropic and several baroclinic components. Figure 1 shows the first five vertical structure functions of the NCEP/NCAR atmosphere, which were obtained numerically using a Galerkin method [*Castanheira et al.*, 1999] between 0 and the mean surface pressure, p_s. However, since the NCEP/NCAR data only extend up to the 10 hPa level, the

vertical structures are not represented above that upper level. The number of nodes (zeros) of a given vertical structure function is equal to the corresponding vertical index m. Since the projection (Eq. 5) onto the barotropic vertical structure, $G_0(p)$, is nearly a vertical average of the atmospheric circulation, it may be regarded as representing the tropospheric circulation [*Castanheira et al.*, 2002]. It is worth noting that all baroclinic modes $m = 2, 3, 4$ have a zero above 10 hPa which is not represented in Figure 1. The first and the second baroclinic structures, respectively $G_1(p)$ and $G_2(p)$, have their nodes in the stratosphere, while the third and the higher vertical baroclinic structure functions have one or more nodes in the troposphere. This feature together with the large amplitude presented by $G_1(p)$ and $G_2(p)$ in the stratosphere make these vertical structure functions especially sensitive to the stratospheric circulation features.

Projections onto the vertical structure functions were then followed by projections onto the horizontal normal modes (Eq. 6), allowing to obtain the complex wave amplitudes, i.e., the coefficients w^{α}_{msl}. Finally the Total energy associated with each planetary Rossby or gravity wave characterized by a given vertical structure m and a given wavenumber s was obtained by summing the energy as given in equation 7 for all meridional indices l.

Although comprehensive studies of normal mode energy spectra may be found in the literature [e.g., *Tanaka and Ji*, 1995, and references therein], we present in Figure 2, for reference purposes, the meridional mean energy spectra for the Rossby modes of wavenumbers $s = 1$, 2 associated with the first three vertical structures. The spectra refer to low frequency waves, i.e. the coefficients were filtered by a 15-day running mean that was applied before computing the energy. The variability spectra, i.e. the spectra

of the standard deviation of intraseasonal or interannual anomalies (not shown) are similar to the respective spectra of the mean energy. The barotropic modes represent the largest amount of energy, in agreement with the fact that they are sensitive to the circulation of the largest fraction of the atmospheric mass, the troposphere. The baroclinic modes $m = 1$, 2 are more sensitive to the lighter layer of atmospheric mass, the stratosphere, and represent smaller amounts of energy. In the lower panel of Figure 2, one may observe the large difference between the energy of wavenumbers $s = 1$ and $s = 2$, which is to be attributed to the wavenumber filtering by the stratosphere.

Finally, it is worth stressing that in the present study, we aim to relate time changes in the energy associated with planetary Rossby waves with the observed vortex variability. Accordingly we have projected the atmospheric circulation onto the first 20 Rossby modes, and results shown in Figure 2 clearly point out that the most important modes were indeed retained in our analysis.

Vortex strength indices

The strength of the polar vortex is represented by means of the stratospheric Northern Hemisphere annular mode (NAM) time series as computed by *Baldwin and Dunkerton* [2001]. The NAM indices, covering the period 1958 to 2001, were obtained from the Baldwin web page (http://www.nwra.com/resumes/baldwin/nam.php).

Mid-winter sudden warming events

Following the WMO definition, a major mid-winter stratospheric warming event occurs when the zonal mean zonal wind at 60° N and 10 hPa becomes easterly, and the gradient

of 10 hPa zonal mean temperature becomes positive between 60° N and 90° N. *Charlton and Polvani* [2006] have developed an objective algorithm to identify SSW events in the extended winter (November to March), based on the sign of the zonal mean zonal wind. The authors have verified that the inclusion of the additional condition on the temperature resulted in a small reduction in the number of detected SSW events. Finally it is worth mentioning that the algorithm is capable of classifying SSW events into those that do and do not split the stratospheric polar vortex.

Table 1 shows the list of SSW events that will be used in the present work as identified in the NCEP/NCAR reanalysis dataset by means of the algorithm developed by *Charlton and Polvani* [2006]. Since we have restricted the computation of daily energies to the periods from November 1 to April 30, and due to the fact that we will have to compute composites starting 35 days before and ending 35 days after the central date of each SSW event, we have excluded from the analysis all events with central dates before December 6 (i.e. one vortex split and two vortex displacements). However, composites computed for shorter time intervals and including the three excluded SSW events led to identical results to the ones that will be presented.

Stratospheric final warming events

Recently *Black et al.* [2006] performed an observational study on the relationship between stratospheric final warming (SFW) events and the Northern extratropical circulation. SFW events were defined as the final time during which the zonal mean zonal wind at 70° N drops below zero without returning to a specified positive threshold value until the subsequent autumn. The criterion was applied to 5-day averages at 10 and 50

hPa with thresholds of 10 and 5 ms^{-1}, respectively.

We will compute composites of daily energies from 40 days before to 20 days after the central dates of each SFW event identified at the 50 hPa level. Event dates were kindly made available by Dr. Robert X. Black and are based on the NCEP/NCAR reanalysis data set covering the 47-year period 1958-2004. The list of SFW events includes 22 earliest events and 22 latest events but our composite analysis will restrict to 19 earliest events, i.e. to those events with central dates earlier than 20 days before April 30. If central dates were chosen up to 10 days before April 30 and composites were built up from 40 days before to 10 days after the central dates of each SFW event, then a set of 30 events would be retained. However we have verified that similar features were obtained with both samples during the common period (i.e. from 40 days before to 10 days after the central dates).

Climatology and anomalies

For every variable, we have removed the respective seasonal cycle, which was estimated by computing at each day the respective inter-annual mean and then by smoothing the obtained time series of daily inter-annual means with a 31-day running average. Daily values of the energy for the total circulation (i.e. climatology + anomaly field) were computed before the seasonal cycle was removed.

On the other hand since we intend to analyse composites of the daily energy during stratospheric events, there is the need to remove the inter-annual components, which for each extended winter was estimated by the respective winter average. Accordingly all anomalies used in our work represent in fact intra-seasonal fluctuations, i.e. departures

from the respective winter averages.

3 Results

Lagged correlations between heat fluxes and wave energy

We have started our analysis by assessing the relationship between the energy and the transport of heat into the stratosphere. It may be worth noting that we have used the heat flux time series averaged between 45° N and 75° N in order to be consistent with the study performed by *Polvani and Waugh* as well as with other previous studies that have considered this same quantity when examining variations in stratospheric wave forcing [*Polvani and Waugh*, 2004, and references therein]. Following these two authors, we performed lagged correlations between Total energy of the planetary Rossby waves and area weighted averages of the meridional eddy heat flux $\overline{v'T'}$ at the 100 hPa level, between 45° N and 75° N. (This time series was kindly made available by Prof. Lorenzo Polvani). Figure 3 shows the obtained lagged correlations between the daily intraseasonal meridional heat flux anomalies and the daily intraseasonal energy anomalies of the barotropic ($m = 0$) and the first two baroclinic ($m = 1$ and $m = 2$) modes of planetary Rossby waves $s = 1$ and $s = 2$. Positive lags mean that the energy is leading. In the case of zonal wavenumber 1 (upper panel), we may observe that the energy anomalies of baroclinic modes $m = 1$ and $m = 2$ are nearly in phase with heat flux anomalies, the energy of $m = 1$ slightly leading and the energy of $m = 2$ slightly lagging the heat flux anomalies. A similar behaviour is apparent in the case of wavenumber 2 (lower panel), albeit the values obtained for the correlations are lower.

Since the heat flux includes contributions from all waves, then the lower correlation values for wavenumber 2 must be due to a larger fraction of the total heat flux with a spatial scale that is associated with wavenumber 1.

In what respects to the barotropic mode $m = 0$ of both planetary Rossby waves $s = 1$ and $s = 2$ the obtained very low values of the correlations are worth being noted, which contrast with the much higher values of the baroclinic modes $m = 1$ and $m = 2$. However this is to be expected since projections onto the barotropic mode mostly reflect tropospheric features of the atmospheric circulation while projections onto the first two baroclinic modes are especially sensitive to the behaviour of the stratospheric circulation.

In summary, obtained results point out that positive (negative) anomalies of the 100-hPa meridional heat flux tend to occur when the Total energy content associated with baroclinic ($m = 1, 2$) planetary Rossby waves $s = 1$ and $s = 2$ is larger (smaller). It may be noted that obtained results are in close agreement with linear wave theory that states that a positive heat flux implies a westward tilt of the wave with height for an upward energy propagation. Hence, the heat flux implies that the wave is baroclinic in structure (i.e. $m \neq 0$).

Lagged correlations between the vortex strength and the wave energy

Limpasuvan et al. [2004, 2005] have shown that the gross behaviour of vortex intensification (VI) events is similar in shape but opposite in sign to the one associated with SSW events. It is therefore natural to analyse vortex forcing by means of lagged correlations between stratospheric NAM indices and wave energy anomalies. A 15-day

running mean was applied to the NAM indices as well as to the total (i.e. climatological + anomaly) atmospheric fields before computing the energy. This procedure was motivated by the known fact that the stratospheric vortex is mainly forced by stationary waves, but similar results were obtained when the 15-running average was applied after computing the energy, an indication of the negligible role played by high frequency waves in the process of vortex intensification.

Results obtained for planetary Rossby waves of wavenumber $s = 1$ are shown in Figure 4, where positive lags mean that the energy is leading. For both baroclinic modes $m = 1$ and $m = 2$ correlation curves indicate that the Total energy oscillates out of phase with the polar night jet. For positive lags, one may also observe that an increase (decrease) of the Total energy of Rossby waves is followed by a weakening (strengthening) of the polar vortex. It is worth stressing that within the context of the wave-mean flow interaction, obtained results are an indication that an increase of the Total energy will be accompanied by an increased wave-1 propagation into the stratosphere, decelerating the jet.

A downward progression of vortex anomalies is also apparent, since the maximum anticorrelation with the NAM index at the 100 hPa level occurs about one week later than the corresponding maximum at the 10 hPa level. Such downward progression is furthermore consistent with the observed lag differences between $m = 1$ and $m = 2$. In fact, as shown in Figure 1, the vertical structure function $m = 1$ represents wind speeds increasing upward in the stratosphere, a vertical profile consistent with the atmospheric state before a warming event. In turn, vertical structure function $m = 2$ represents wind speeds decreasing in the upper stratosphere, and such profile is consistent with the

developing phase of a warming event[*Kodera et al.*, 2000, Fig. 2]. If vertical structure functions are multiplied by -1, then the same reasoning may be valid when applied to VI events. Finally it is worth noting that the observed oscillatory behaviour in the correlation curves for $s = 1$ and $m = 1,\ 2$ closely agrees with the findings by *Limpasuvan et al.* [2004] (see their Figure 10d), and further suggests a stratospheric vacillation cycle [*Kodera et al.*, 2000].

As already pointed out, the linear wave theory suggests that the vertical wave propagation depends on both the zonal and the meridional wave numbers [*Andrews et al.*, 1987]. However the lagged correlations that are depicted in Figure 4 refer to the sum of the energy of all meridional modes. In order to assess the effects due to the meridional scales we computed the lagged correlations between the energy of each Rossby mode and the vortex strength at the same stratospheric levels. Figure 5 shows the obtained largest correlations or anticorrelations as a function of the meridional index of the Rossby modes. It should be noted that the considered positive (negative) lags lie inside the time intervals where the maximum anticorrelations (correlations) in Figure 4 were found , i.e. the considered positive (negative) lags are contained by the interval where curves in Figure 4 are marked by solid (open) circles. It is well apparent that the larger meridional scales (i.e. the smaller meridional indices) are the only ones that significantly interact with the vortex strength. As negative correlations were obtained when the energy is leading the vortex strength (i.e. with positive lags) and therefore represent a forcing of the vortex strength, it may seem awkward that the magnitude of the anticorrelation is smaller for meridional indices $l = 0,\ 1,\ 2$. However such behaviour is readily understood if we take into account that the largest values (weights)

of the first meridional structures do locate at lower latitudes than those associated with high meridional indices. In fact, since the weights of the meridional structures at high latitudes increase as the meridional index increases [Longuet-Higgins, 1968], meridional modes $l = 0, 1, 2$ ($l = 3, ..., 6$) are more sensitive to the atmospheric circulation at lower (higher) latitudes. The meridional Rossby mode $l = 8$ of the second baroclinic structure also presents a conspicuous positive correlation for positive lags, but positive energy anomalies in this mode may be also associated with an upscale energy transfer to the modes which forces the vortex. This possibility is in agreement with the results in Figure 6 that show an anticorrelation at lag 0 between the energy associated with the meridional mode $l = 8$ and the energy associated with modes $l = 2, 3, 4, 5$. However validating such an hypothesis requires further research work.

As pointed out above, positive correlations in Figure 4 may reflect a stratospheric vacillation (see also Figure 6), but since the vortex strength is leading such positive values may also be due to some other effect of the vortex. In this respect, we note that the obtained maximum correlation for $s = 1$ and $m = 1$ (upper panel in Fig. 5) occurs for meridional indices $l = 1$ and 2, a feature that may be the result of equatorward wave refraction during the strong vortex period.

SSW events

As specified in Table 1, we have separately analyzed the energy composites for SSW events of the displacement and splitting types and it is worth noting that both composites respect to daily intraseasonal anomalies without any smoothing. Figure 7 shows the composite for SSW events of the displacement type and it is apparent that such

events are preceded by a period of about one month of statistically significant (at the 5% level) positive anomalies of the energy associated with the baroclinic modes $m = 1$ and $m = 2$ of zonal wavenumber 1. Circa one week after the event's central date the baroclinic component $m = 1$ presents statistically significant (at the 5% level) negative anomalies that remain until the end of the study period. A general positive trend may be observed in the barotropic component ($m = 0$) of wavenumber 2, and a general negative trend is apparent in the barotropic component of zonal wavenumber 1. These results are consistent with the findings by *Charlton and Polvani* [2006] for the composites of meridional heat flux.

It is worth noting that the statistical significance of anomalies in the energy composites was assessed by means of 1,000 random composites. Each composite was built up by randomly choosing 13 central dates (day 0) from the winter period between the earliest observed SSW event and the latest one. For each composite day the 2.5, 5, 95 and 97.5 percentiles were determined from the 1,000 random samples. Solid (open) symbols in composite curves denote points which are below the 2.5 (5) or above the 97.5 (95) percent levels and therefore represent anomalies that are statistically significant at the 5% (10%) level. Data multiplicity was taken into account by building up a new set of 1,000 random composites and then evaluating the percentage of composites with a statistically significant (at the 5% level) number of days larger than the observed ones. Table 2 shows the obtained percentages which are separately given for the positive and the negative anomalies. Cases where the percentage of random composites is smaller than 5% are shown in boldface.

As shown in Figure 8, composites for SSW events of the split type suggest a differ-

ent dynamics from the ones of the displacement type. In this case both wavenumbers 1 and 2 seem to play an important role and a precursor of such events, associated with positive (negative) energy anomalies of the baroclinic $m = 1$ (barotropic $m = 0$) components of zonal wavenumber 1, seems to take place during the period from about 30 to 15 days before the central date. It may be possible that early wavenumber 1 energy anomalies are associated with a deceleration of the stratospheric jet, setting the conditions for wavenumber 2 propagation into the polar region. However, the present analysis cannotrule out the possibility of a downscale energy transfer due to nonlinear wave interactions. Following such preconditioning, SSW events of split type evolve with an increase of energy associated with the barotropic and the baroclinic components of wavenumber 2, during a period of about 15 days before the event central's date. Afterwards, the baroclinic components of both wavenumbers 1 and 2 present statistically significant (at the 5% confidence level) negative anomalies. Finally, the observed drastic change in the sign of anomalies of the barotropic component of wavenumber 2, from negative to positive lags, is particularly worth noting since it gives an indication of drastic changes in the energetics of the tropospheric circulation before and after the central dates of SSW events of the split type. This results agrees with those of *Nakagawa and Yamazaky* [2006] who have shown that during the growth stage of SSW events that propagate into the troposphere, there is an enhanced upward flux of energy associated with wavenumber 2. Obtained results also support the findings of *Charlton and Polvani* [2006], but it is worth stressing that our analysis points to the possible different nature of the tropospheric impacts by SSW events of the displacement and split types.

Table 3 shows the statistical significance of the composites of SSWs of split type

taking into account data multiplicity.

SFW events

Figure 9 presents the energy composites that were obtained for the considered set of 19 earliest SFW events having occurred before April 11. In case of zonal wavenumber 1, it is well apparent that SFW events are preceded by statistically significant (at the 10% level) positive energy anomalies of the first two baroclinic components ($m = 1, 2$), which concentrate into two distinct periods of time. This feature is in strong agreement with the findings of *Black et al.* [2006] who have identified two periods of strong vortex deceleration (see their Figure 2) that coincide with two distinct bursts of upward Eliassen-Palm flux (see their Figure 3). In particular it is worth noting that the observed positive anomaly of the second baroclinic Rossby mode during the second deceleration period (i.e. the time interval where the anomalies of $m = 2$ are the only statistically significant ones) is also in agreement with the results of *Black et al.* [2006]. Indeed, the second deceleration period in their Figure 2 is characterised by easterly zonal mean zonal wind in the upper stratosphere and westerly zonal wind in the lower stratosphere, a vertical structure that is well captured by the baroclinic component $m = 2$. The statistical significance of the SFW composites is shown in Table 4.

Finally, a comparison of figures 7 and 9 suggests that the wave dynamics of SFW events presents some similarities with the one of SSW events of the displacement type. Both events seem to be forced by means of an increase of energies associated with the baroclinic Rossby modes ($m = 1, 2$) of planetary wavenumber 1. Positive anomalies of the energy are observed during the 30 days before the events, and there is a trend of

the energy associated with the barotropic Rossby mode of wavenumber 1 to decrease during the evolution of the events.

4 Concluding remarks

In this work we have looked at the problem of the variability of the stratospheric polar vortex from the point of view of planetary wave energetics. Our analysis differs from traditional methods in that we have concentrated on a diagnosis of the energy associated with the forcing waves instead of analysing Eliassen-Palm fluxes. Another difference from previous studies relates to the fact that instead of being restricted to the extratropical subdomain, our analysis is applied to the whole atmosphere, and the relevant circulation components are selected by means of projections onto 3-D global functions that allow partitioning the atmospheric (global) circulation into planetary Rossby waves and inertio-gravity waves with barotropic and baroclinic vertical structures.

We have found that positive (negative) anomalies of the energy associated with the first two baroclinic Rossby modes $m = 1$ and $m = 2$ of planetary wave $s = 1$ are followed by downward progression of negative (positive) anomalies of the vortex strength. A signature of the vortex vacillation is also apparent in the lagged correlation curves between wave energy of individual Rossby modes and vortex strength. Obtained values of correlations further confirm the result from linear theory that the waves which force the vortex are those associated with the largest meridional scales.

Composite analysis of stratospheric sudden warming (SSW) events of the displacement and the split types have revealed different dynamics. SSW events of the displace-

ment type are forced by positive anomalies of the energy associated with the first two baroclinic Rossby modes $m = 1$ and $m = 2$ of planetary zonal wavenumber $s = 1$. On the other hand, SSW events of the split type are forced by positive anomalies of the energy associated with planetary zonal wavenumber $s = 2$. Besides, the barotropic Rossby component of wavenumber $s = 2$ has revealed a strong anomaly signal of opposite sign before and after the central date of the event, suggesting that the tropospheric circulation plays a important role in the activation of SSW events of the split type, and that, after the events, anomalies propagate down to the troposphere [*Nakagawa and Yamazaky* , 2006]. In the case of SSW events of the split type, a preconditioning of the stratospheric circulation seems to take place three weeks before the event as suggested by the observed behaviour of the anomalies of the baroclinic Rossby modes of zonal wavenumber $s = 1$.

In the case of stratospheric final warming (SFW) events, obtained results closely agree with the findings of *Black et al.* [2006] and there is evidence that composites of SFW events exhibit an overall similar behaviour to the one observed in composites of SSW events of the displacement type.

Acknowledgements. Dr. Laura de La Torre had received a grant from the University of Vigo to visit the University of Aveiro.

References

Andrews, D. G., J. R. Holton e C. B. Leovy, 1987. *Middle Atmosphere Dynamics.* Academic Press, 489 pp.

Baldwin, M. P., and T. J. Dunkerton, 1999: Propagation of the Arctic Oscillation from the stratosphere to the troposphere. *J. Geophys. Res.,* **104,** 30 937-30 946.

Baldwin, M. P., and T. J. Dunkerton, 2001: Stratospheric harbingers of anomalous weather regimes. *Science,* **294,** 581-584.

Black, R. X., B. A. McDaniel, and W. A. Robinson, 2006: Stratosphere-troposphere coupling during spring onset. *J. Climate,* 19, 4891-4901.

Castanheira, J. M., C. C. DaCamara and A. Rocha, 1999: Numerical solutions of the vertical structure equation and associated energetics. *Tellus,* **51A,** 337-348.

Castanheira, J. M., H.-F. Graf, C. DaCamara and A. Rocha, 2002: Using a Physical reference frame to study Global Circulation Variability. *J. Atmos. Sci.,* **59,** 1490-1501.

Charlton, A. J., and L. M. Polvani, 2006: A new look at stratospheric sudden warmings. Part I. Climatology and modelling benchmarks. *J. Climate,* (in press).

Daley, R., 1991: *Atmospheric data analysis.* Cambridge University Press, 457 pp.

Hartmann, D. L., J. M. Wallace, V. Limpasuvan, D. W. J. Thompson, and J. R. Holton, 2000: Can ozone depletion and global warming interact to produce rapid climate change? *PNAS,* **97** (4), 1412-17.

Holton, J. R., H.-C. Tan, 1980: The influences of the equatorial quasi-biennal oscillation on the global circulation at 50 mb. *J. Atmos. Sci.,* **37,** 2200-2208.

Kalnay, E. et al., 1996: The NCEP/NCAR 40-year reanalysis project. *Bull. Amer. Meteor. Soc., 77,* 437-471.

Kodera, K., and Y. Kuroda, 2000: A mechanistic model study of slowly propagating coupled stratosphere-troposphere variabiliy. *J. Geophys. Res.,* **105,** 12 361-12 370.

Kodera, K., Y. Kuroda, and S. Pawson, 2000: Stratospheric sudden warmings and slowly propagating zonal mean zonal wind anomalies. *J. Geophys. Res.,* **105,** 12 351-12 359.

Labitzke, 1982: On the interannual variability of the middle stratosphere during the northern winters. *J. Meteor. Soc. Japan,* **60,** 124-139.

Limpasuvan, D. W. J. Thompson, and V., D. L. Hartmann,2004: The life cycle of the Northern Hemisphere sudden stratospheric warmings. *J. Climate,* **17,** 2584-25-96.

Limpasuvan, V., D. L. Hartmann, D. W. J. Thompson, K. Jeev, and Y. L. Yung, 2005: Stratosphere-troposphere evolution during polar vortex intensification. *J. Geophys. Res.,* **110,** doi:10.1029/2005JD006302

Longuet-Higgins, M. S., 1968: The eigenfunctions of Laplace's tidal equations over a sphere. *Phil. Trans. Roy. Soc., London,* **A262,** 511-607.

McDaniel, B. A., and R. X. Black, 2005: Intraseasonal dynamical evolution of the Northern Annular Mode. *J. Climate,* **18,** 3820–3839.

Naito, Y., M. Taguchi, and S. Yoden, 2003: A parameter sweep experiment on the effects of the equatorial QBO on stratospheric sudden warmings events. *J. Atmos. Sci.,* **60,** 1380-1394.

Nakagawa, K. I, and K. Yamazaky, 2006: What kind of stratospheric sudden warming propagates to the troposphere? *Geophys. Res. Lett.,* **33,** doi:1029/2005GL024784.

Perlwitz, J. and N. Harnik, 2004: Downward coupling between the stratosphere and troposphere: The relative roles of wave and zonal mean processes. *J. Climate,* **17,** 4902–4909, doi:10.1175/JCLI-3247.1.

Polvani, L. M., and P. J. Kushner, 2002: Tropospheric response to stratospheric perturbations in a relatively simple general circulation model. *Geophys. Res. Lett.,* **29,** doi:10.1029/2001GL014284.

Polvani, L. M. and D. W. Waugh, 2004: Upward wave activity flux as a precursor to extreme stratospheric events and subsequent anomalous surface weather regimes. *J. Climate,* **17,** 3548–3554.

Song, Y. and W. A. Robinson, 2004: Dynamical mechanisms for stratospheric influences on the troposphere. *J. Atmos Sci.,* **61,** 1711–1725.

Tanaka, H. L., 2003: Analysis and Modeling of the Arctic Oscillation Using a Simple Barotropic Model with Baroclinic Eddy Forcing. *J. Atmos. Sci.,* **60,** 1359-1379.

Tanaka, H. L., and Q. Ji, 1995: Comparative energetics of FGGE Re-analyses using the normal mode expansion. *J. Meteor. Soc., Japan,* **73,** No. 1, 1-12.

Thompson, D. W. J., M. P. Baldwin, and J. M. Wallace, 2002: Stratospheric connection to Northern Hemisphere wintertime weather: Implications for predictions. *J. Climate 15,* 1421–1428.

Thuburn, J., and V. Lagneau, 1999: Eulerian mean, contour integral, and finite-amplitude wave activity diagnostics applied to a single-layer model of the winter stratosphere. *J. Atmos. Sci.,* **56,** 689-710.

List of Figures

1. Vertical structure functions of the barotropic $m = 0$ and the first 4 baroclinic modes ($m = 1, \ldots, 4$) of the NCEP/NCAR atmosphere. It is worth noting that the NCEP/NCAR database only extends up to the 10 hPa level.

2. Winter (November to March) mean energy of the Rossby modes with wavenumbers $s = 1$, 2 associated with the barotropic structure $m = 0$ (top) and the baroclinic structures $m = 1$, 2 (bottom). In the lower panel, solid (dashed) curves refer to $s = 1$ ($s = 2$).

3. Lagged correlations between daily intraseasonal anomalies of planetary Rossby wave energy and daily intraseasonal anomalies of area-weighted means of meridional eddy heat flux $\overline{v'T'}$ at the 100 hPa level, between 45° N and 75° N. Upper and lower panels respect to zonal wavenumbers $s = 1$ and $s = 2$, respectively. Positive lags mean that the energy is leading.

4. Lagged correlations at 6 stratospheric levels between NAM indices and wave energy for wavenumber $s = 1$ of the baroclinic Rossby modes $m = 1$ (upper panel) and $m = 2$ (lower panel). Solid (open) circles identify lags of maximum anticorrelation (correlation). Positive lags mean that the energy is leading.

5. Lagged correlations between the energy of each Rossby mode and the NAM indices at the same stratospheric levels as in Figure 4. Solid (dashed) curves show the largest anticorrelations or correlations for positive (negative) lags inside the time interval where the maximum anticorrelations (correlations) in Figure 4 are found,

i.e. in the interval where the solid (open) circles are shown. Upper (lower) panel refers to baroclinic structure $m = 1$ ($m = 2$) of wavenumber $s = 1$.

6. Time change in energy associated to Rossby modes with wavenumber $s = 1$ and baroclinic structure $m = 2$. Solid line represents the autocorrelation of the sum of energy associated with meridional indices $l = 2, 3, 4, 5$. Dashed line represents the lagged correlations between the sum of energy of the same meridional indices and the energy of the Rossby mode with meridional index $l = 8$.

7. Daily composites of intraseasonal anomalies of wave energy for SSW events of the displacement type. Day 0 refers to the central date of the event. Solid (open) symbols identify mean values of intraseasonal anomalies that statistically differ from zero at the 5% (10%) significance level (see text).

8. As in Figure 7 but respecting to SSW events of the split type.

9. As in Figure 7 but respecting to SFW events.

Table 1: List of stratospheric sudden warming (SSW) events that were considered in this work. SSW events were identified in the NCEP/NCAR dataset based on the algorithm developed by *Charlton and Polvani* [2006]. Letters D and S in the second column identify SSW events of the displacement and of the split types respectively. ΔT refers to area-weighted means of the polar cap temperature anomaly at the 10 hPa level, during periods from 5 days before up to 5 days after the central dates of each event.

central date	type	ΔT (K)	central date	type	ΔT (K)
30/01/1958	S	7.8	29/02/1980	D	11.5
16/01/1960	D	5.9	24/02/1984	D	11.1
23/03/1965	S	4.4	02/01/1985	S	13.0
08/12/1965	D	6.7	23/01/1987	D	10.2
24/02/1966	S	3.1	08/12/1987	S	14.1
08/01/1968	S	12.0	14/03/1988	D	11.7
13/03/1969	D	4.3	22/02/1989	S	12.8
02/01/1970	D	6.8	15/12/1998	D	12.7
17/01/1971	S	9.6	25/02/1999	S	11.0
20/03/1971	D	-2.9	20/03/2000	D	5.3
02/02/1973	S	6.6	11/02/2001	D	6.3
22/02/1979	S	3.7	02/01/2002	D	12.9

Table 2: Percentages of random composites which have a number of statistically significant (at 5% level) positive (negative) anomalies greater than the obtained number of statistically significant positive (negative) anomalies in the observed composite of SSW events of the displacement type. Cases where the percentage of random composites is smaller than 5% are shown in boldface.

	Positive anomalies			Negative anomalies		
	$m = 0$	$m = 1$	$m = 2$	$m = 0$	$m = 1$	$m = 2$
$s = 1$	100	**0.0**	**0.0**	100	**0.7**	6.0
$s = 2$	100	100	100	38.3	100	100

Table 3: As in Table 2 but for the SSW events of the split type.

	Positive anomalies			Negative anomalies		
	$m = 0$	$m = 1$	$m = 2$	$m = 0$	$m = 1$	$m = 2$
$s = 1$	53.7	**1.3**	20.9	38.0	**0.0**	**4.1**
$s = 2$	**2.1**	**0.8**	**1.0**	**2.7**	9.9	**0.1**

Table 4: As in Table 2 but respecting to SFW events.

	Positive anomalies			Negative anomalies		
	$m = 0$	$m = 1$	$m = 2$	$m = 0$	$m = 1$	$m = 2$
$s = 1$	35.2	**1.5**	**0.2**	18.0	**5.0**	5.8
$s = 2$	100	17.8	100	10.2	40.5	100

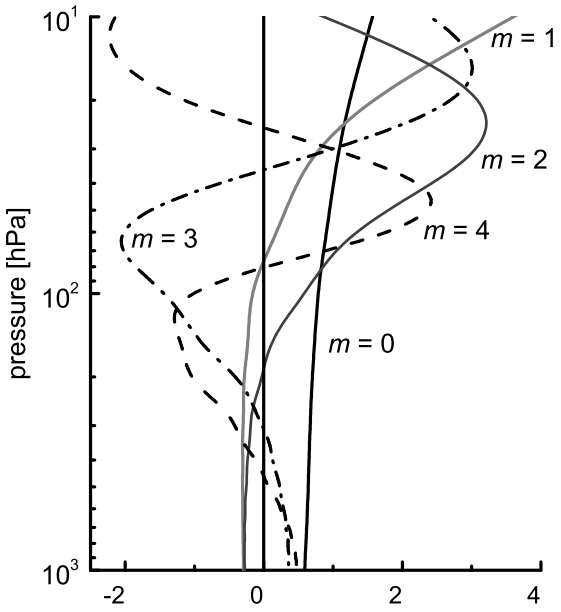

Figure 1: Vertical structure functions of the barotropic $m = 0$ and the first 4 baroclinic modes ($m = 1, \ldots, 4$) of the NCEP/NCAR atmosphere. It is worth noting that the NCEP/NCAR database only extends up to the 10 hPa level.

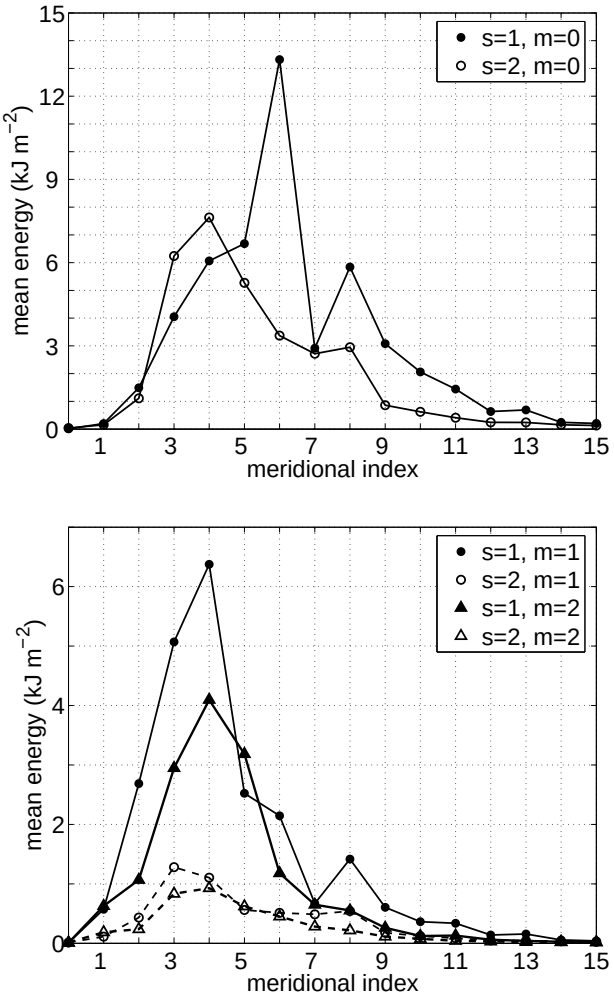

Figure 2: Winter (November to March) mean energy of the Rossby modes with wavenumbers $s = 1, 2$ associated with the barotropic structure $m = 0$ (top) and the baroclinic structures $m = 1, 2$ (bottom). In the lower panel, solid (dashed) curves refer to $s = 1$ ($s = 2$).

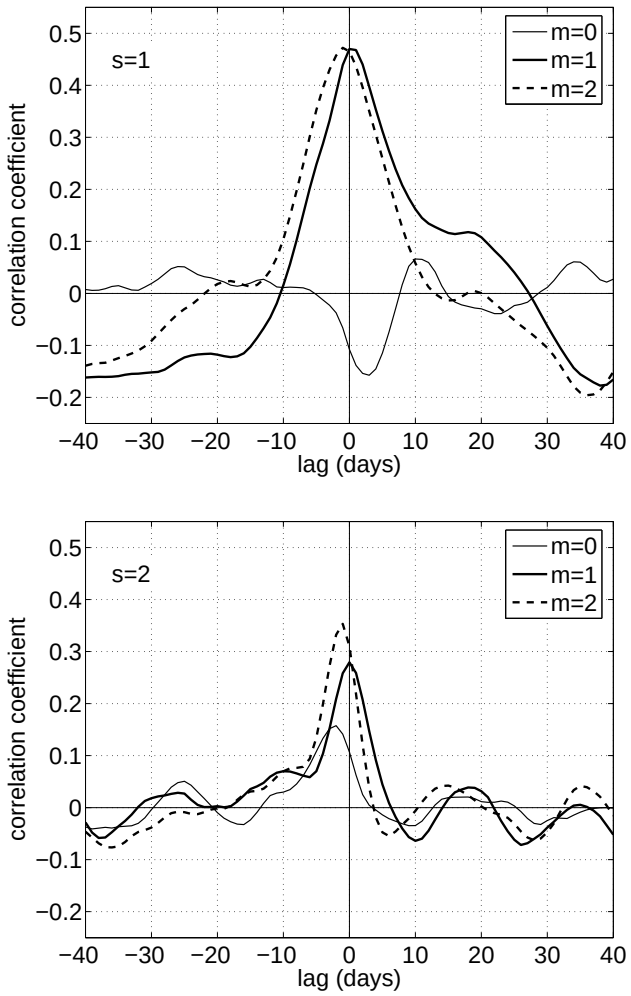

Figure 3: Lagged correlations between daily intraseasonal anomalies of planetary Rossby wave energy and daily intraseasonal anomalies of area-weighted means of meridional eddy heat flux $\overline{v'T'}$ at the 100 hPa level, between 45° N and 75° N. Upper and lower panels respect to zonal wavenumbers $s = 1$ and $s = 2$, respectively. Positive lags mean that the energy is leading.

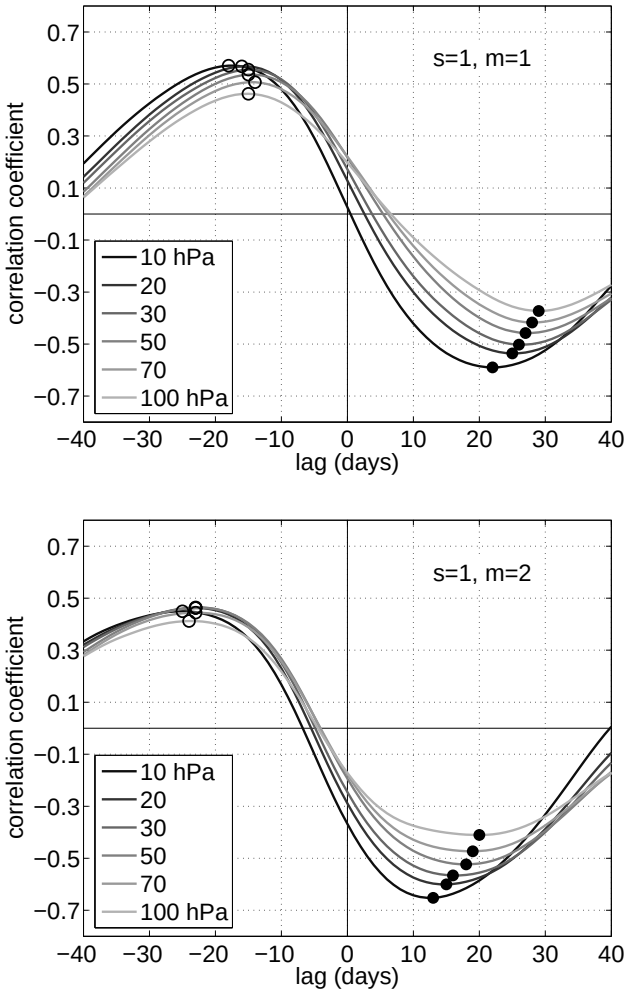

Figure 4: Lagged correlations at 6 stratospheric levels between NAM indices and wave energy for wavenumber $s = 1$ of the baroclinic Rossby modes $m = 1$ (upper panel) and $m = 2$ (lower panel). Solid (open) circles identify lags of maximum anticorrelation (correlation). Positive lags mean that the energy is leading.

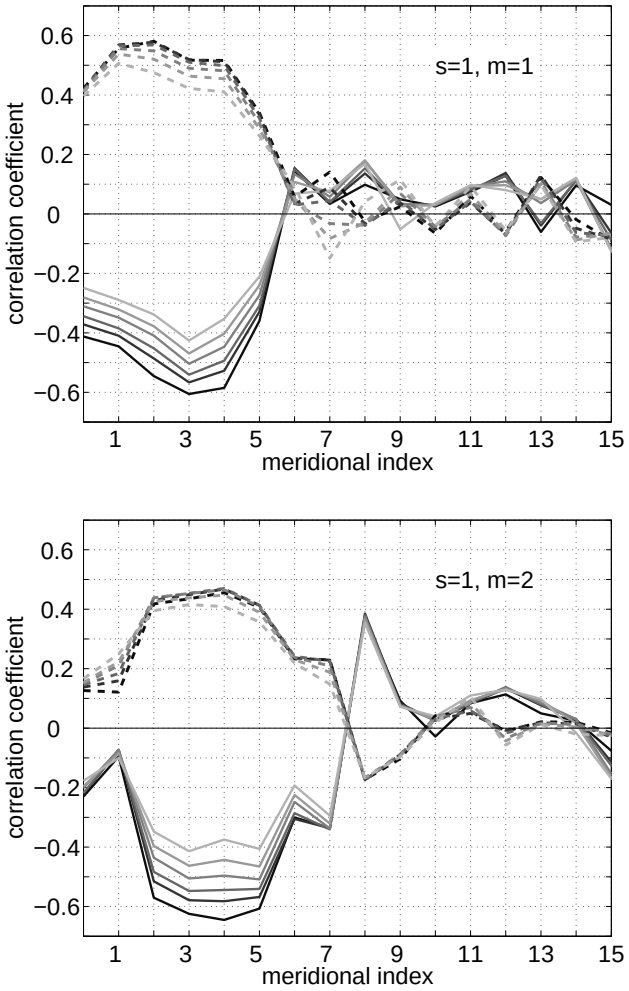

Figure 5: Lagged correlations between the energy of each Rossby mode and the NAM indices at the same stratospheric levels as in Figure 4. Solid (dashed) curves show the largest anticorrelations or correlations for positive (negative) lags inside the time interval where the maximum anticorrelations (correlations) in Figure 4 are found, i.e. in the interval where the solid (open) circles are shown. Upper (lower) panel refers to baroclinic structure $m = 1$ ($m = 2$) of wavenumber $s = 1$.

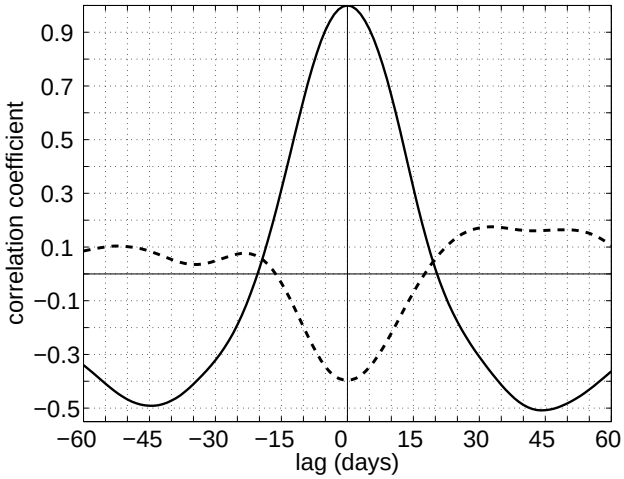

Figure 6: Time change in energy associated to Rossby modes with wavenumber $s = 1$ and baroclinic structure $m = 2$. Solid line represents the autocorrelation of the sum of energy associated with meridional indices $l = 2, 3, 4, 5$. Dashed line represents the lagged correlations between the sum of energy of the same meridional indices and the energy of the Rossby mode with meridional index $l = 8$.

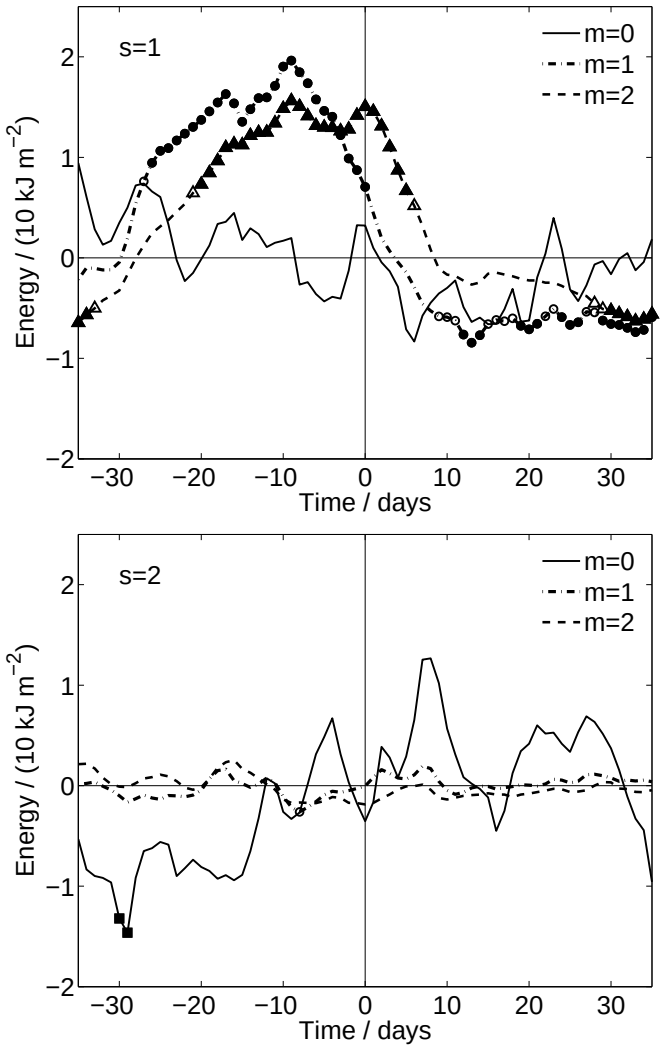

Figure 7: Daily composites of intraseasonal anomalies of wave energy for SSW events of the displacement type. Day 0 refers to the central date of the event. Solid (open) symbols identify mean values of intraseasonal anomalies that statistically differ from zero at the 5% (10%) significance level (see text).

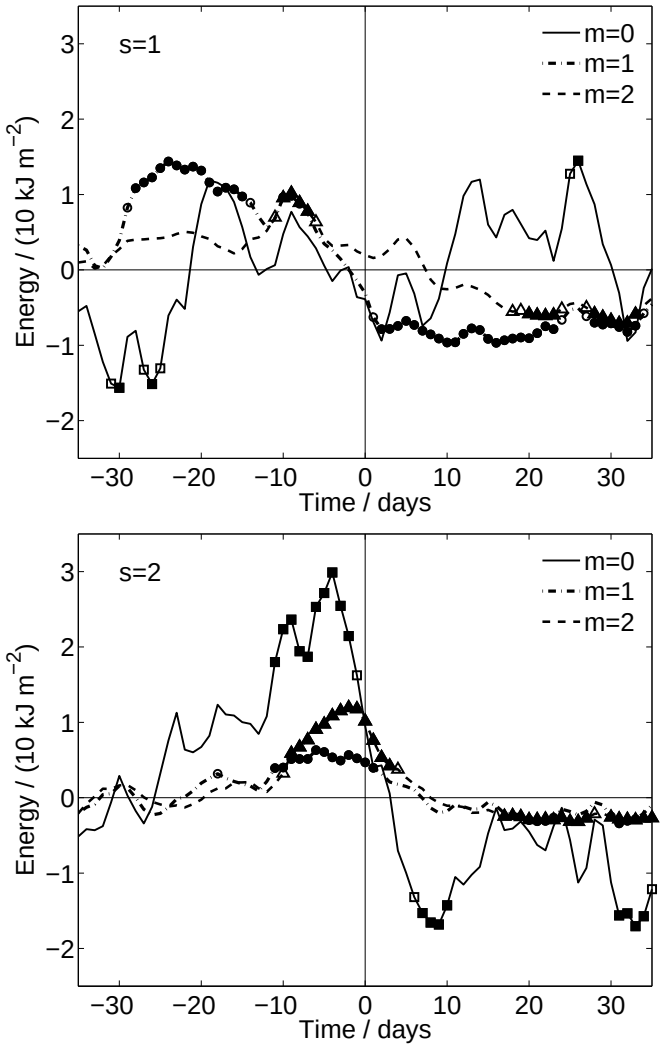

Figure 8: As in Figure 7 but respecting to SSW events of the split type.

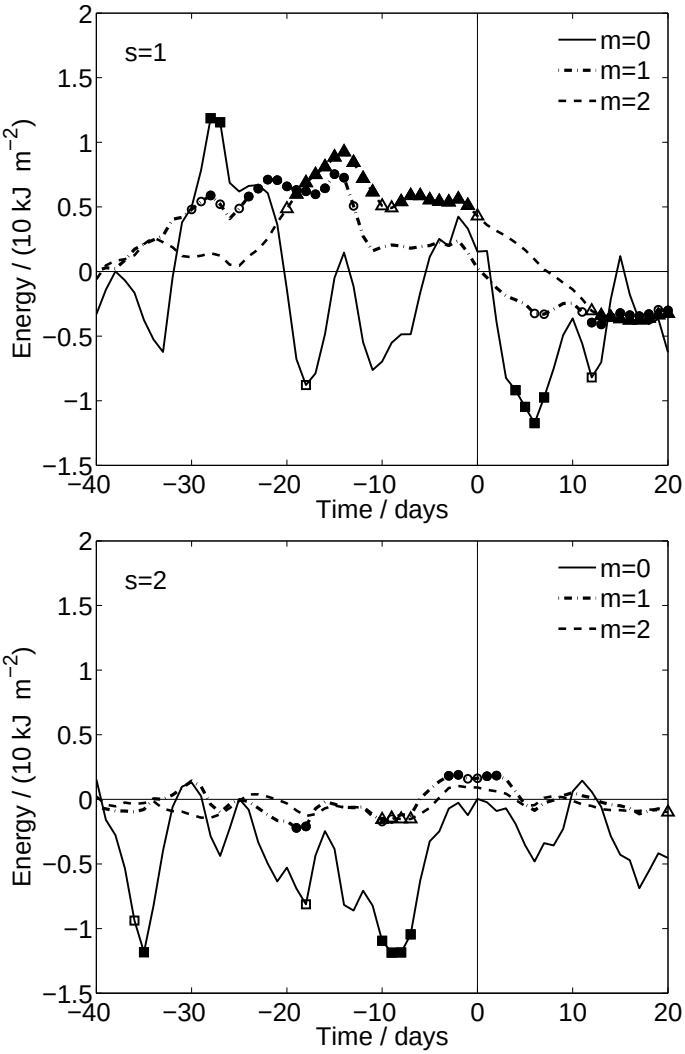

Figure 9: As in Figure 7 but respecting to SFW events.